Journal of Alloys and Compounds 372 (2004) 224–230

Journal of ALLOYS AND COMPOUNDS

www.elsevier.com/locate/jallcom

Nanomechanical properties of nanocrystalline Ni–Fe mold insert

Y.-M. Yeh [a,*], G.C. Tu [a], T.-H. Fang [b]

[a] *Department of Materials Science and Engineering, National Chiao Tung University, Hsinchu 300, Taiwan*
[b] *Department of Mechanical Engineering, Southern Taiwan University of Technology, Tainan 710, Taiwan*

Received 10 January 2003; accepted 30 August 2003

Abstract

Nanocrystalline Ni–Fe alloy micro-mold inserts were fabricated by UV lithographic technology and pulse current electroforming process. The structure, surface and mechanical properties of Ni–Fe alloys were evaluated under different pulse current electroforming processes via X-ray diffraction (XRD), scanning probe microscope (SPM), nanoindentation, and scanning transmission electron microscope (STEM). The results show that when Fe content of the alloys increase by over 10% the grain size of Ni–Fe alloys was <20 nm. The finer the grain of Ni–Fe alloys the higher the hardness, which is above 9 GPa. By controlling the variation of current density and duty cycle, the surface roughness of Ni–Fe alloys is <10 nm and the surface friction coefficient is about 0.2. The results of the microelectroforming process revealed that the Fe contents was able to suppress grain growth and induced the formation of dense Ni–Fe alloys and improved the mechanical properties of the Ni–Fe alloys.

Keywords: Ni–Fe alloy; Electroforming; Surface friction coefficient; Nanoindentation

1. Introduction

Recently MEMS technology has been successfully applied to the fabrication of many tips such as microsensor, microgears, microactuators [1–3]. The LIGA (or LIGA-like) process which contains lithography, electroforming, and molding is one of the most important microfabrication technologies to fabricate high aspect ratio 3D microstructures. Hence, microelectroforming is an important process in microfabrication. Many materials for LIGA (or LIGA-like) have been investigated [4–10]. Among them, many new metals and alloy materials such as Au, Cu, Ni and Ni–Fe are able to been used to manufacture microelectroforming applications. The Ni–Fe alloys have been widely considered for both scientific and practical applications due to their properties such as low thermal expansion, high magnetic permeability, excellent structural-quality and their mechanical properties. Various compositions of Ni–Fe alloys such as, Permalloy (80Ni–20Fe), Invar alloy (36Ni–64Fe) and high strength Ni–Fe alloy can be used to produce microsensor, microactuators and other MEMS device. Hence, the mechanical and the surface properties of nanocrystalline Ni–Fe alloys by microelectroforming in LIGA process are worth studying.

In microelectroforming process, the applied current form and current density will affect microstructure and mechanical properties. Previous studies found that pulse current electroforming has better characteristics on nickel-based alloy deposition [11–17]. Pulse electroforming not only has uniform composition, but also reduced the anomaly of Ni–Fe [12,14]. In addition, smooth surface, fine-grained structure and lower internal stress can be controlled by various current waveforms and pulse frequency [13,17,18]. Ni electroforming has been used in LIGA (or LIGA-like) extensively in the previous studies [4,19–24]. Only a few studies have discussed about Ni–Fe alloys electroforming in LIGA (or LIGA-like) [5,7,25,26]. A relatively small number of investigations have measured and reported values for the Young's modulus, surface roughness and hardness of LIGA (or LIGA-like) Ni–Fe microcomponent [27,28].

In order to progress in the analyses of microelectroforming mold insert and gain microcomponents characteristics the properties of Ni–Fe alloys by microelectroforming are necessary. In this study, an electroforming stencil is prepared by SU-8 photoresist and UV-light exposure technology. Various high aspect ratio mold inserts of Ni–Fe alloys

* Corresponding author. Tel.: +886-3-571-2121; fax: +886-3-572-6111.

0925-8388/$ – see front matter © 2003 Elsevier B.V. All rights reserved.
doi:10.1016/j.jallcom.2003.08.101

Table 1
Composition and condition of Ni–Fe alloy electroforming solution

Description	Concentration
Nickel sulfate (g/l)	200
Iron sulfate (g/l)	8
Nickel chloride (g/l)	5
Boric acid (g/l)	40
Saccharin (g/l)	3
Sodium lauryl sulfate (g/l)	0.5
Pulse current density (J_m, mA/cm^2)	20–80
pH	3 ± 0.2
Temperature (°C)	50

are prepared by pulse current electroforming. Nanocrystalline characteristics of Ni–Fe alloys are evaluated by X-ray diffraction (XRD), scanning probe microscope (SPM), nanoindentation, and scanning transmission electron microscope (STEM). Additionally the fractal dimension and nanofriction are employed to investigate the surface of Ni–Fe alloys.

2. Experimental procedures

2.1. SU-8 lithography process

The substrates used in these experiments were p-type (1 0 0) oriented silicon wafers with resistivity of 5–10 μΩ cm. The Si wafers were cleaned in a dilute HF solution (HF:H_2O = 1:20) for 2 min, and rinsed in de-ionized water. 100–150 μm SU-8 photoresist was spin-coated on Si substrate after the RCA cleaning process. Soft backing, exposure, post exposure backing, develop processes were performed successively. The 200 nm Cu films were deposited at a power of 500 W in a sputtering system using a sputtering pressure of 6.4 m Torr after the base pressure was evacuated to below 5×10^{-7} Torr.

2.2. Ni–Fe microelectroforming process

In this study, a 10 l electroplating tank was use to performed electroforming. The power supply was controlled by potentiostat/golvanostat (EG&G 263) and Head Start software (provided by EG&G). The chemicals and operation conditions are shown in Table 1.The pulse electroforming consisted of duty cycle (i.e. pulse on time dived by pulse on time plus pulse off time) between 0.3 and 0.7. In the pretreatment process of electroforming, plating cell, rack, anode basket and S–Ni anode must be cleaned. In addition, in order to decrease the internal stress of micro-mold insert, weak electrolysis treatment with low current density is performed for 12 h to remove metal ions and an active carbon filter is used to filter organic impurities to decrease the defects in the coating layers.

2.3. Property measurements of microelectroforming Ni–Fe alloys

In order to realize the relationship of microstructure and mechanical properties, microstructure of Ni–Fe alloy was observed using scanning transmission electron microscopy (STEM). Electron microscopy was performed on a transmission electron microscope (TEM, JEOL 2000FX, Japan) operating at 200 kV. Plan-view TEM samples were prepared by mechanical thinning to 3 μm followed by ion milling to electron transparency which was performed by precision ion polishing system (PIPS) with the bombardment of 4 kV Ar ions and the samples were maintained at room temperature. Transmission electron microscopy was used for grain size examination. Grazing incidence X-ray diffractometry (GIXRD) was carried out for crystalline preferred orientation and calculation of grain size. The crystallographic structure of the alloys was examined by X-ray diffraction (XRD) analysis with a Cu Kα source. The current and voltage were 40 mA and 50 kV, respectively. To enhance the sensitivity for X-rays, the measurements were performed in parallel beam geometry at a constant incident angle of $\alpha = 2^\circ$. The registered angle range was $2\theta = 20$–80° with a step size $\Delta G\theta = 0.02^\circ$ and a measuring time of 1 s per step.

A nanoindentation technique is used to measure hardness and Young modulus of Ni–Fe alloys. It not only analyzed the relationship of the force and depth in real time but also gained high precision results. The nanoindentation experiments were performed using the Hysitron triboscope (Hysitron, USA). A diamond Berkovich indenter with a tip radius of 60 nm is forced into the material being investigated. In this study the indentation testing followed a trapezoidal loading profile with a hold time of typically 10 s at a loading rate of 10 μN/s. Surface morphology and surface friction coefficient were measured by scanning probe microscope (SPM, Shimadzu SPM-9500J2, Tokyo, Japan) to observe the specimens. A constant scan speed of 1 m/s is used and a constant load is applied to the V-type cantilever which had a pyramidal tip made of Si_3N_4 with a tip radius of about 15 nm [29].

3. Results and discussion

3.1. Nanocrystalline Ni–Fe alloy microstructure

Fig. 1 plots the XRD pattern of Ni–Fe alloys using microelectroforming process. As shown in Fig. 1, The as-deposited Ni–Fe alloys have polycrystalline structure and a (1 1 1) preferred orientation peak is obvious. Mechanical properties of Ni–Fe layer are related with preferred orientation. The different current densities and power supply styles used affected the crystallographic texture. Based on Cheung et al. [30] previous study, the intensity of (2 0 0) oriented peak decreased as Fe contents increased. The nanocrystallinization effect was also obvious with increasing Fe contents. In

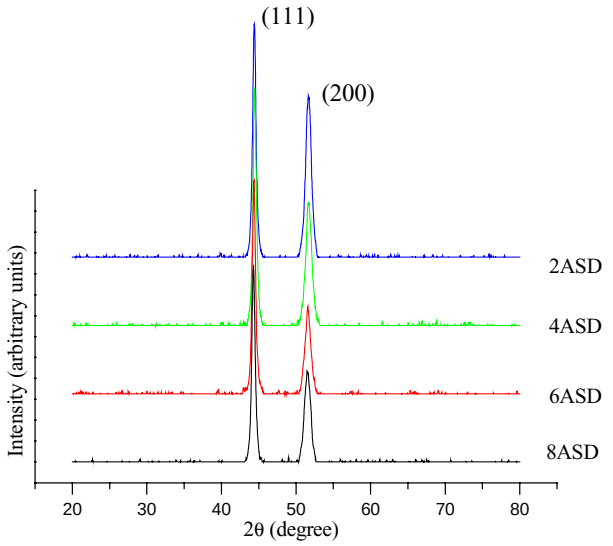

Fig. 1. X-ray diffraction pattern of Ni–Fe alloy at different current densities.

other words, Fig. 1 shows that increasing the current density induces the nanocrystallization and amounts of Fe precipitation. In order to realize the relationship of pulse current density and grain size of electroforming layers, Scherrer equation is used for the calculation of the mean crystalline size D from the full-width at half maximum (FWHM). The grain sizes decreased as current density increased. Variation of grain sizes is from 15 to 11 nm, implying that nanocrystallization occurs due to current density variation. Fig. 2 displays dark field TEM micrograph of Ni–Fe alloys with various current densities. It can be seen from Fig. 2(a) and (b) that the grain size is about 17 nm using a low current density of 2ASD. The grain size is slightly smaller in the Ni–Fe alloy that undergoes higher current density. Dark field images of Fig. 2(c) and (d) have smaller grains (13 nm) as the current density is increased to 8ASD. The results of the TEM and XRD experiments are in strong agreement with each other.

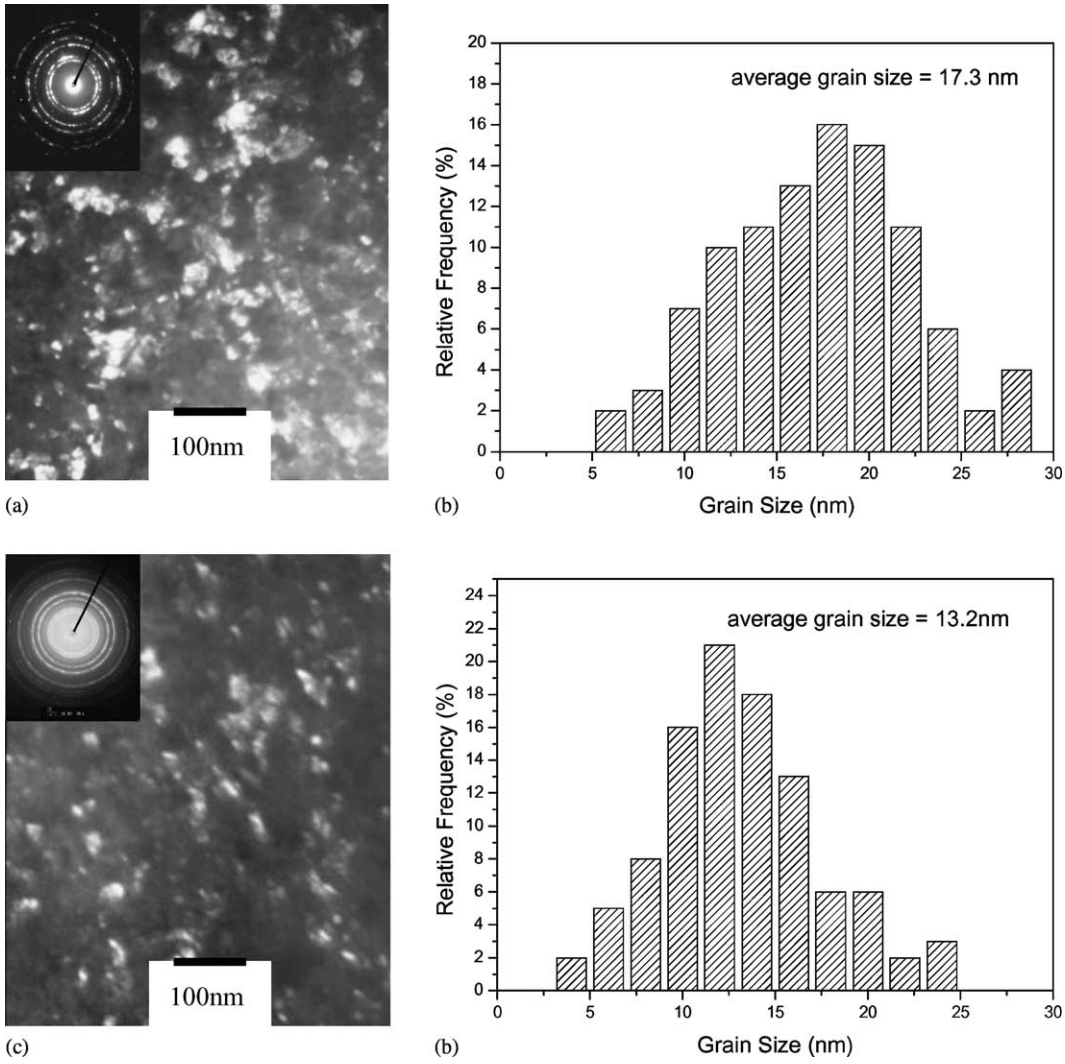

Fig. 2. TEM micrographs for electroforming nanocrystalline Ni–Fe alloy (left: dark-field and electron diffraction pattern; right: grain size distribution): (a) and (b) 2ASD; (c) and (d) 8ASD.

3.2. Surface morphology and roughness

It was reported that the use of pulse (reverse) current resulted in the nickel formation of deposit with better surface finishing than that formed by direct current [31–34]. In addition, overhang phenomenon can be avoided in controlling pulse electroplating [35]. Based on the investigation, pulse current has better step coverage than that of direct current in high aspect ratio microelectroforming mold. High aspect ratio structure can be obtained at various duty cycles in electroforming, which improves the yield of the mold insert. Surface morphology and surface roughness of mold insert is very important in molding process. In order to gain high aspect ratio and better form translation, excellent surface roughness of micro-mold insert must be required. Fig. 3 shows AFM images of Ni–Fe alloys mold insert at various current densities with a constant 0.5 operation period. It shows that a better surface is observed at the current density of 6ASD. It reveals the nucleation rate is lower than the growth rate at lower current densities. High deposition rate induces defects such as microtwin and microstrain.

In addition, various duty cycles will also affect the surface roughness as shown in Fig. 4 and shows that less surface roughness is obtained at the mid level operating period (duty cycle). The long relaxation period (off time) allows metal atom to have a long diffusion time in cathode reaction. It also reveals that as an operating period at 0.5 and pulse current density of 4–6ASD produces a smoother surface morphology.

3.3. Fractal analysis

Fractal analysis is used to investigate the surface engineering that significantly simplifies the morphology analysis of surface properties on Ni–Fe alloys. Fractal surface maintains the characteristics of continuity, self-similar, non-differentiability and self-affine. By definition, a fractal is a set for which the so-called fractal dimension, D_s, always exceeds the topological dimension. In this methodology, the fractal dimension is calculated from the least-square degeneration line of a log–log plot of structure function $S(\tau)$ versus a large vector τ [36].

The results of fractal dimension Ni–Fe mold insert at various operating current densities are shown in Fig. 5 and indicate that the fractal dimension is approximately 2.15–2.20 and has a lower complicated geometry. The surface morphology varies slightly at various operating conditions. It means that pulse electroforming possesses better surface stability characteristics and can be operated in broad ranges for every electroforming parameter. Fig. 5 plots the higher

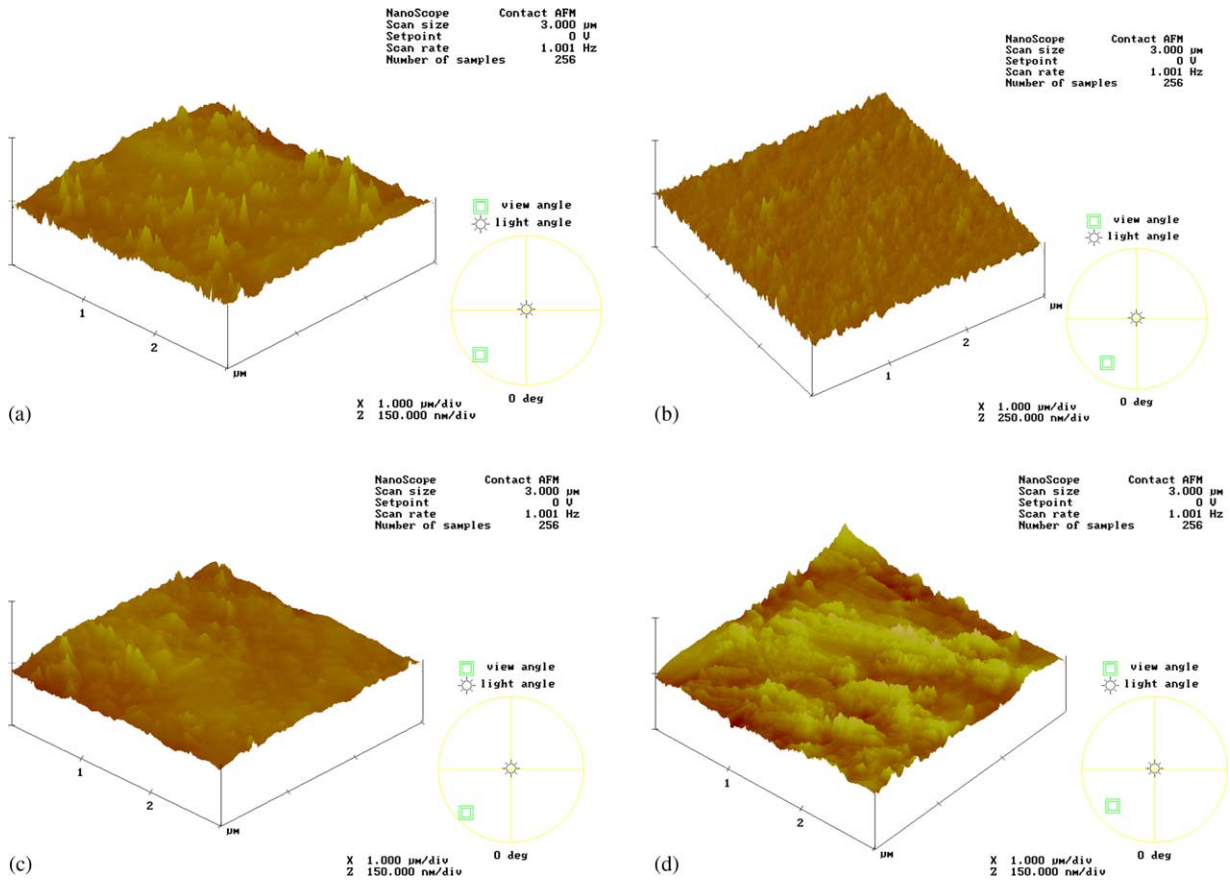

Fig. 3. 3D AFM image of electroforming Ni–Fe mold insert at different current densities: (a) 2ASD; (b) 4ASD; (c) 6ASD; (d) 8ASD.

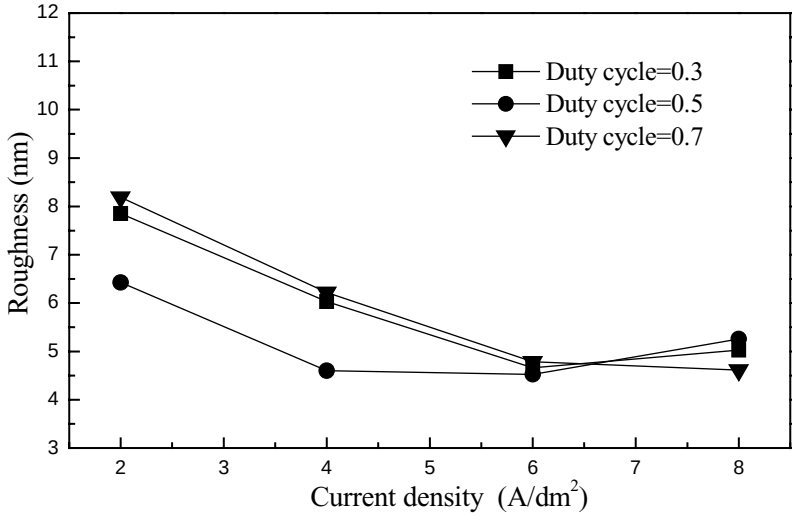

Fig. 4. The effect of current densities on the surface roughness of electroforming Ni–Fe mold insert.

fractal dimension and is observed in dc electroforming compared with pulse electroforming. The lowest fractal dimension value is detected in 6ASD pulse electroforming and is in agreement with the analysis of surface roughness, although, fractal dimension may not be related with surface roughness. It is obvious fractal dimension is proportional to surface roughness in pulse electroforming, however, the dc electroforming does not observed the relationship like the pulse electroforming. At various operating periods in pulse current electroforming, the cathode provides an off time. The off time induces Ni and Fe atoms to have enough time to diffuse into surface defects. The lower fractal dimension is obtained at a duty cycle of 0.5 and current density of 6ASD as seen in Fig. 5.

3.4. Friction test

The friction coefficient is defined as the average ratio of friction force to the normal force or the slope of the curve

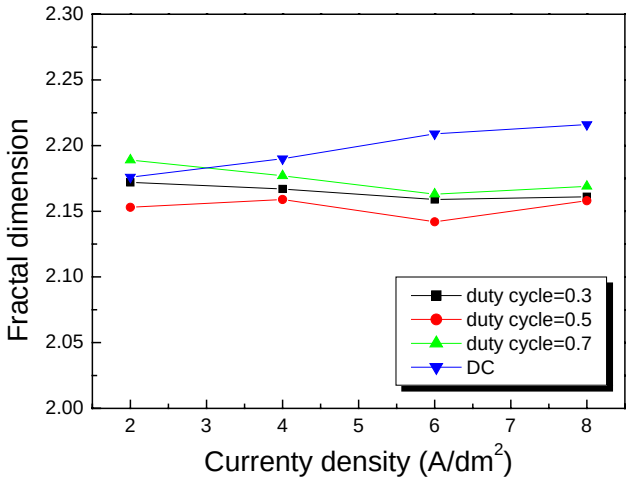

Fig. 5. The effect of current densities on the fractal dimension of electroforming Ni–Fe mold insert.

generated by the plotting friction force and normal load. The relationship of friction coefficient and the scanning size is shown in Fig. 6. The friction coefficient of Ni–Fe alloy is approximately 0.2 at the nanofriction test. For comparison with the macro-friction, a ring to disk wear test is performed as the conventional method. Its results show that the average friction coefficient is about 0.4–0.6 in the same electroforming. It reveals the microstructure possesses low friction coefficient. This similar result was also investigated by other research [37]. The friction coefficient as detected by SPM is lower than the macro-friction.

3.5. Hardness and Young's modulus

Many moving microcomponents of MEMS such as microgear, microactuator, etc need acceptable static or dynamics stress so they must possess enough mechanical strength and stiffness. It is important that microhardness and Young's modulus of Ni–Fe alloy be revealed by nanoindentation technique. Young's modulus is calculated using the effective elastic modulus, E_{eff}, which is taken by [38]:

$$E_{\text{eff}} = \frac{1}{2}\sqrt{\frac{\pi}{A_{\text{c}}}}\frac{\mathrm{d}P}{\mathrm{d}h} \tag{1}$$

where $\mathrm{d}P/\mathrm{d}h$ is the slope of the unloading curve and A_{c} the projected contact area at the maximum load. The final Young's modulus, E, is obtained from the expression:

$$\frac{1}{E_{\text{eff}}} = \frac{1-\nu^2}{E} + \frac{1-\nu_i^2}{E_i} \tag{2}$$

where the material properties E_i is 1141 GPa and ν_i 0.07 for a diamond indenter and $\nu = 0.27$ for the Ni–Fe alloys.

Fig. 7 shows load–displacement curves for Ni–Fe alloys under various current densities. It can be seen that the stiffness of high current density electroforming Ni–Fe alloys is higher than that of low current density. Fig. 8 shows the relationship of hardness and Young's modulus at different

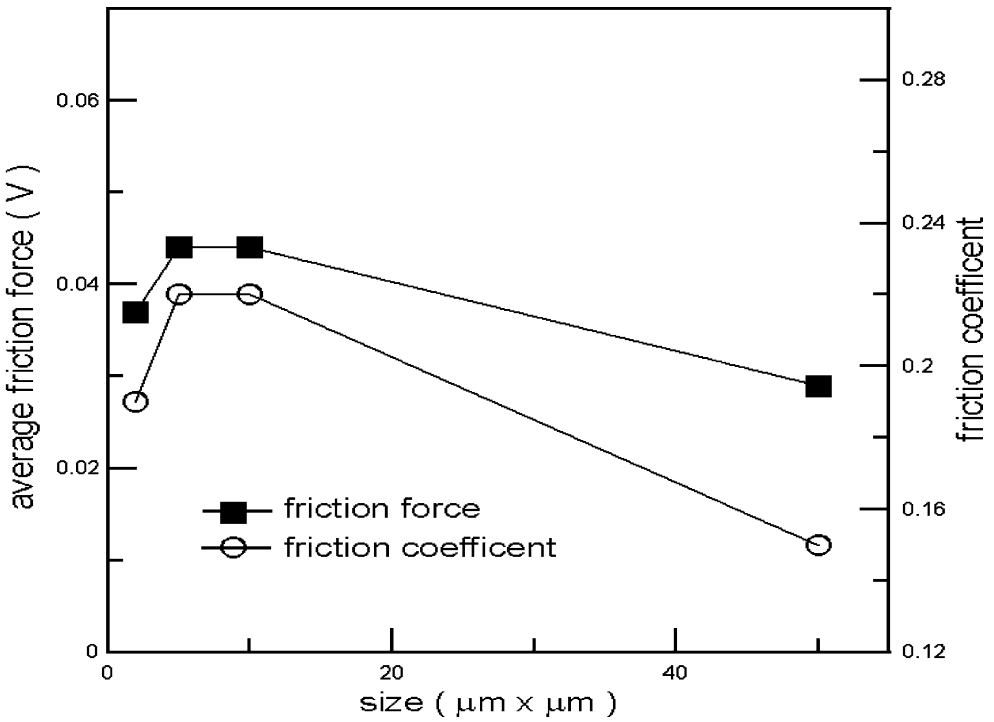

Fig. 6. Friction force and coefficient of the Ni–Fe alloy micro-mold insert.

current densities. Both Young's modulus and hardness increases as the current density increases. It reveals that as current density increases, nanocrystallization is observed in electroforming. The nanocrystallization effect increases hardness. The finer the grain of Ni–Fe alloys the higher the hardness, which is above 9 GPa. In addition, as current density increases the amounts of Fe-precipitation increase, which resulted in increased hardness. High current density induces formation of Ni–Fe alloys having (1 1 1) preferred crystallographic orientation and caused higher hardness. This effect of texture on the hardness of nanocrystalline Ni-based materials had been reported earlier on other researchers [30,39,40]. In addition, Fig. 8 shows that as current density increases, Young's modulus of Ni–Fe alloy increases. The phenomenon is the reason that increasing current density results in nanocrystallization. The Young's modulus of Ni nano-grains prepared by electrodeposition is ~125–214 GPa. The difference is affected by the coating solution. Watts bath is higher that the sulfamate bath [24]. In comparison with electroforming, the grain size of Ni–Fe alloy is about 15 nm. Young's modulus of Ni–Fe alloys is 316 GPa. It reveals that nanocrystallization effect and alloy strengthing give rise to the promotion of mechanical property.

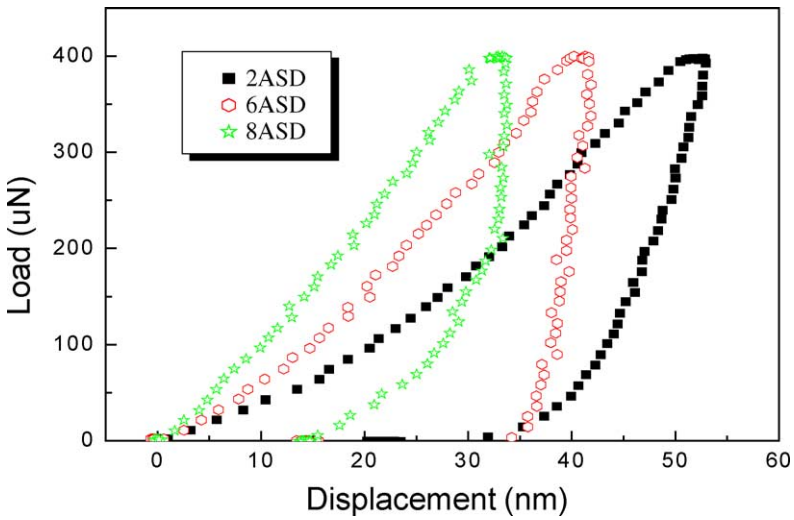

Fig. 7. Nanoindentation load–depth curves for various shapes in nanocrystalline Ni–Fe alloy.

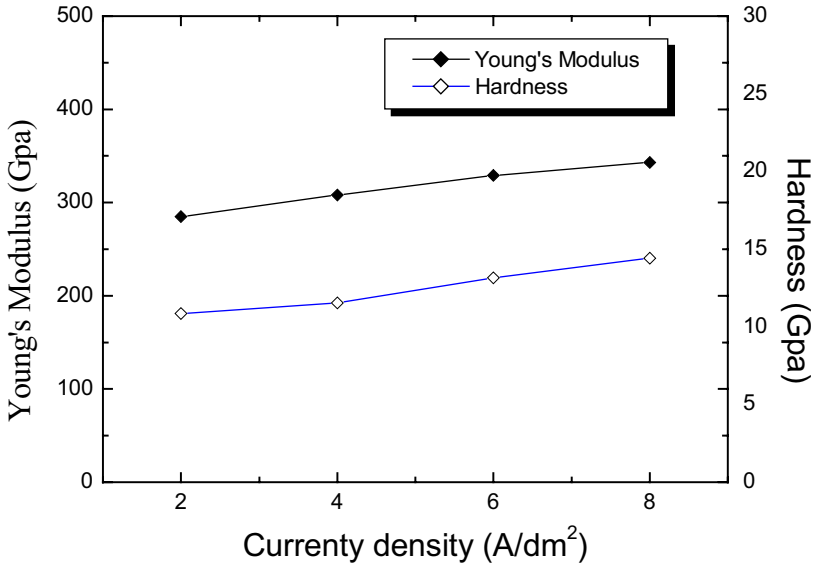

Fig. 8. The effect of current densities on the Young's modulus of electroforming Ni–Fe mold insert.

4. Conclusions

The mechanical properties of nanocrystalline Ni–Fe alloys were evaluated under different pulse current electroforming process. The results indicated that a finer grain of Ni–Fe alloys exhibits a higher hardness. The hardness is above 9 GPa and Young modulus is approximately 316 GPa. The surface roughness of Ni–Fe alloys is <10 nm and surface friction coefficient is about 0.2 by controlling the current density and duty cycle. A finer grain of Ni–Fe alloys can induce formation of dense Ni–Fe alloys and improve mechanical properties of Ni–Fe alloys.

References

[1] J. Bryzek, Sens. Actuators A 56 (1996) 1.
[2] T. Hirano, L.S. Fan, J.Q. Gao, W.Y. Lee, J. Microelectromechan. Syst. 7 (1998) 149.
[3] D.J. Nagel, M.E. Zaghloul, IEEE Circuits Dev. 17 (2001) 14.
[4] E.W. Becker, W. Ehrfeld, P. Hagmann, A. Maner, D. Münchmeyer, Microelectron. Eng. 4 (186) 35.
[5] B. Löchel, A. Maciossek, H.J. Quenzer, B. Wagner, J. Electrochem. Soc. 143 (1) (1996) 237.
[6] A. Bruno Frazier, M.G. Allen, J. Microelectromechan. Syst. 2 (1993) 87.
[7] J. Gobet, F. Cardot, J. Berqvist, F. Rudolf, J. Micromech. Microeng. 3 (1993) 123.
[8] A. Maciossek, B. Löchel, H.J. Quenzer, B. Wanger, S. Schulze, J. Noetzel, Microelectron. Eng. 27 (1995) 503.
[9] M.C. Chou, H. Yang, S.H. Yeh, Microsyst. Technol. 7 (2001) 36.
[10] W. Ehrfeld, M. Abraham, U. Ehrfeld, M. Lacher, H. Lehr, Proc. IEEE Microelectromechan. Syst. (1994) 86.
[11] N. Ibl, Surf. Technol. 10 (1980) 81.
[12] J.C. Puippe, F. Leaman, Theory and Practice of Pulse Plating, AESF, Orlando, FL, 1986.
[13] Y.N. Sadana, Z.H. Zhang, Surf. Coat. Technol. 38 (1989) 299.
[14] D.L. Grimmett, M. Schwartz, K. Nobe, J. Electrochem. Soc. 137 (1990) 3414.
[15] K.M. Yin, S.L. Jan, C.C. Lee, Surf. Coat. Technol. 88 (1996) 219.
[16] P.E. Bradley, D. Landolt, Electrochim. Acta 42 (1997) 993.
[17] K.C. Chan, W.K. Chan, N.S. Qu, J. Mater. Proc. Technol. 89–90 (1999) 447.
[18] K.P. Wong, K.C. Chan, T.M. Yue, Surf. Coat. Technol. 115 (1999) 132.
[19] H. Majjad, S. Basrour, P. Delobelle, M. Schmidt, Sens. Acturators 74 (1999) 148.
[20] S. Abel, H. Freimuth, H. Lehr, H. Mensinger, J. Micromech. Microeng. 4 (1994) 47.
[21] W. Daniau, S. Ballandras, L. Kubat, J. Hardin, G. Martin, S. Basrour, J. Micromech. Microeng. 5 (1995) 270.
[22] J. Fahrenberg, T.H. Schaller, W. Bacher, A. EI-Kholi, W.K. Schomburg, Microsyst. Technol. 2 (1996) 174.
[23] S. Roth, L. Dellmann, G.A. Racine, N.F. De Rooij, J. Micromech. Microeng. 9 (1999) 105.
[24] L.S. Stephens, K.W. Kelly, S.S. Simhadri, A.B. McCandless, E.I. Meletis, J. Microelectromechan. Syst. 10 (2001) 347.
[25] S.P. Bäckstrom, C. Riekel, S. Abel, H. Lehr, H.R. Wenk, J. Appl. Cryst. 29 (1996) 118.
[26] S.D. Leith, D.T. Schwartz, J. Microelectromechan. Syst. 8 (1999) 384.
[27] E. Mazza, S. Abel, J. Dual, Microsyst. Technol. 2 (1996) 197.
[28] J.T. Ravnkilde, V. Ziebart, O. Hansen, H. Baltes, Sens. Mater. 12 (2000) 99.
[29] T.H. Fang, C.I. Weng, J.G. Chang, C.C. Hwang, Thin Solid Films 396 (2001) 166.
[30] C. Cheung, F. Djuanda, U. Erb, G. Palumbo, Nanostruct. Mater. 5 (1995) 513.
[31] T.P. Sun, C.C. Wan, Y.M. Shy, Met. Finishing 77 (1979) 33.
[32] S. Abel, H. Freimuth, H. Lehr, H. Mensinger, J. Micromech. Microeng. 4 (1994) 47.
[33] M. Saitou, W. Oshikawa, M. Mori, A. Makabe, J. Electrochem. Soc. 148 (2001) C780.
[34] N.S. Qu, K.C. Chan, D. Zhu, Surf. Coat. Technol. 91 (1997) 220.
[35] C.Y. Lee, A. Krishnamoorthy, D.J. Duquette, W.N. Gill, J. Electrochem. Soc. 147 (2001) 3382.
[36] N. Almgvist, Surf. Sci. 355 (1996) 221.
[37] W. Wang, Y. Wang, H. Bao, B. Xiong, M. Bao, Sens. Acturators A 97–98 (2002) 486.
[38] W.C. Oliver, G.M. Pharr, J. Mater. Res. 7 (1992) 1564.
[39] G. McMahon, U. Erb, Microstruct. Sci. 17 (1989) 447.
[40] A.F. Zimmerman, G. Palumbo, K.T. Aust, U. Erb, Mater. Sci. Eng. A 328 (2002) 137.